



Eidgenössische Technische Hochschule Zürich
Swiss Federal Institute of Technology Zurich

Analysis of the Photodegradation of Gold Nanorods in Optoacoustic Imaging

Bachelor Thesis

Jérôme Bonvin

Tuesday 30th December, 2025

Advisors: Prof. Dr. Daniel Razansky, Dr. Xosé Luís Deán-Ben

Department of Electrical Engineering, ETH Zürich

Abstract

In this thesis, we investigated the performance of AuNRs as optoacoustic contrast agents. The study assessed the influence of wavelength, energy, and number of pulses on the optoacoustic signal and morphology of AuNRs. The results demonstrated a complex interplay between these factors, with varying effects on the signal intensity, degradation rate, and morphological stability of the nanoparticles. Moreover, an algorithm was developed to segment AuNRs in Scanning Electron Microscope (SEM) images and to quantify their dimensions.

The study highlights the importance of AuNRs in optoacoustic imaging and the need for further research to fully harness their potential. The thesis concludes that a better understanding of the factors affecting AuNR behavior is crucial for optimizing their use in medical imaging and developing more effective and reliable contrast agents.

Contents

Contents	ii
1 Introduction	1
2 Theoretical Model	3
2.1 Initial Pressure Rise	3
2.2 Optoacoustic Signal Generation	4
3 Synthesis of Gold Nanoparticles	6
3.1 Determination of the type of Nanoparticle	6
3.2 Synthesis of the Gold Nanorods	7
3.3 Synthesis of the Bi-Pyramidal Nanoparticles	8
3.3.1 Filtering	9
4 Optoacoustic Setup	10
4.1 Laser Setup	10
4.2 Ultrasound Cup Setup	12
5 Coding and Results	15
5.1 Getting the Data	15
5.2 Fitting the Data	18
5.3 Results and Discussion	19
6 SEM Imaging analysis	24
6.1 Particle Detector App	25
6.2 Image Processing	25
6.3 Results of SEM Analysis	26
7 Conclusion	29
Bibliography	30

Chapter 1

Introduction

Optoacoustics, also known as photoacoustic imaging, is a rapidly growing field that combines the principles of optics and acoustics to create a powerful imaging modality with a wide range of applications. In optoacoustics, light is used to excite a photoabsorbing material, such as gold nanoparticles, which generates ultrasound waves due to the rapid temperature increase induced by the light absorption. These ultrasound waves can then be detected using ultrasound transducers, creating a high-resolution image of the underlying distribution of the photoabsorbing material.

Optoacoustics offers several advantages over traditional imaging modalities, such as ultrasound and optical imaging. It is non-invasive and does not require ionizing radiation, making it ideal for medical applications. Additionally, optoacoustics can provide high spatial and temporal resolution, allowing for the visualization of small structures and rapid processes.

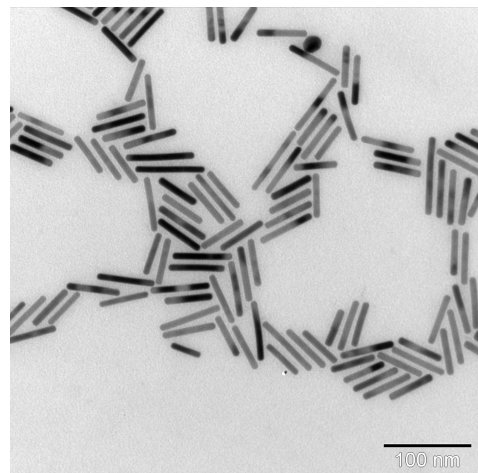


Figure 1.1: TEM image of Gold Nanorods

AuNR associated to photodegradation is not fully understood, and it is important to study this process in order to improve their performances.

The OA signal decay of AuNRs is a complex process that is influenced by several factors, including the energy density of the excitation light, the wavelength of the light, and the amount of time¹ at which the AuNRs are exposed to the light.

Energy Dependency:

The decay rate of AuNRs is generally found to increase with increasing energy density of the excitation light. This is because higher energy light photons can more readily excite electrons in the AuNRs, leading to a faster loss of optical absorption and a shorter lifetime.

Wavelength Dependency:

The decay rate of AuNRs can also be affected by the wavelength of the excitation light. In general, AuNRs absorb light more efficiently at specific wavelengths, and the OA signal for those wavelengths tends to decay faster.

Our research aims to investigate the effects of these factors on the OA signal decay of AuNRs in optoacoustic imaging. Our goal is to contribute to a better understanding of the OA signal decay process of AuNRs and to use this understanding to improve the performance of optoacoustic imaging and other AuNR-based applications.

¹In this thesis, time is often referred as the number of pulses that an object will receive, this is because there are 10 pulses of laser every second.

Chapter 2

Theoretical Model

Before diving into the practical details of measuring the optoacoustic signal from gold nanorods (AuNRs), it is crucial to establish a theoretical framework to guide our experiments and provide a baseline for interpretation of the results. In this chapter, we will explore the fundamental principles of optoacoustic signal generation and apply them to our specific case of AuNRs. This theoretical foundation [1] will serve as a roadmap for our experimental investigations.

2.1 Initial Pressure Rise

Before going into the formulas, some assumptions ought to be considered. The laser used for this project is a short pulsed laser that emit light pulses of about 10ns . We also assume that the duration of this pulse is shorter than the stress relaxation time and than the thermal relaxation time. The optoacoustic signal generation process is straightforward. When a laser pulse illuminates a tissue, it rapidly absorbs the light energy, converting it into heat. This localized heating causes an expansion and contraction due to its expansion coefficient. This phenomenon generates ultrasound waves that propagate through the tissue. These ultrasound waves can be detected by transducers, which convert the acoustic energy back into electrical signals. These electrical signals can then be processed and analyzed to reconstruct an image of the tissue's optical absorption distribution.

The initial pressure rise is a crucial parameter in optoacoustic imaging, as it directly influences the amplitude of the generated acoustic waves. This pressure rise arises from the rapid expansion of a small volume of tissue in response to a localized heat source. The change in volume, represented by ΔV , is governed by both temperature T and pressure p . When a volume of tissue absorbs light, it gains energy, which is transformed into heat, causing

2.2. Optoacoustic Signal Generation

the temperature to rise. This increase in temperature leads to a corresponding expansion of the tissue, resulting in a pressure increase.

$$\frac{\Delta V}{V} = \frac{1}{V} \frac{\delta V}{\delta T} |_p \Delta T + \frac{1}{V} \frac{\delta V}{\delta p} |_T \Delta p \approx 0$$

The relative variation of volume is approximately 0 since we assume that the tissue that we are imaging is an incompressible fluid. Therefore we can find the relation:

$$\Delta p = p_0 = \frac{\beta}{\kappa_T} \Delta T$$

where $\beta = \frac{1}{V} \frac{\delta V}{\delta T} |_p$ is the thermal expansion coefficient for gold and $\kappa_T = \frac{1}{V} \frac{\delta V}{\delta p} |_T$ is the isothermal compressibility for gold.

$$\begin{aligned} \Delta T &= \frac{1}{C_v} Q = \frac{1}{C_v} \mu_a \varphi \\ \Rightarrow p_0 &= \frac{\beta}{\kappa_T C_v} \mu_a \varphi = C \mu_a \varphi \end{aligned}$$

where C_v is the volumetric heat capacity, Q is the heat per unit volume, μ_a is the absorption coefficient and φ is the fluence.

To focus on the behavior of the variable terms, we simplified the constant terms in the equations by representing them with a single constant C . This approach allowed us to isolate and analyze the influence of the variable terms on the optoacoustic signal, without being hindered by the complexities of the constant values. This simplification provided a clearer understanding of the relationship between the variable parameters and the generated acoustic waves.

2.2 Optoacoustic Signal Generation

To further analyze the optoacoustic signal, we investigated how it behaves when the particles produce multiple pressure rises over time. In our experiments, this time dependency is directly related to the number of laser pulses that the AuNRs receive. As the AuNRs are exposed to multiple laser pulses, they undergo a process of degradation, which can be approximated by an exponential decay function $e^{-\alpha_\lambda t}$, where α_λ is a positive number that represents the rate of decay for a given wavelength.

Combining this time dependence with the initial pressure rise equation, we obtain:

$$p_0(\lambda, t) = C \mu_a(\lambda, t) \varphi(\lambda, t) e^{-\alpha_\lambda t}$$

where $\mu_a(\lambda, t)$ represents the wavelength-time-dependent absorption coefficient of the AuNRs. It's important to note that the absorption spectrum is

2.2. Optoacoustic Signal Generation

not linearly affected by time. Instead, the peak of the spectrum may become flattened and shifted towards lower wavelengths as the AuNRs undergo degradation, causing them to lose their rod-like shape and become more spherical. This shift in the absorption spectrum is attributed to the change in the AuNRs' morphology, which alters their interaction with light and affects their optical absorption characteristics.

In conclusion, the theoretical model presented in this chapter provides a solid foundation for understanding the optoacoustic signal generation process and its dependence on wavelengths. The initial pressure rise equation, which relates the pressure rise to the laser fluence and the absorption coefficient, highlights the crucial role of absorption in generating acoustic waves. The time-dependent optoacoustic signal model further demonstrates how the absorption coefficient of the AuNRs affects the amplitude of the acoustic waves over time. By incorporating the effects of AuNR degradation and morphological transformation, this model provides a comprehensive understanding of the factors that influence the degradation of optoacoustic signal.

Chapter 3

Synthesis of Gold Nanoparticles

The synthesis of gold nanoparticles (AuNRs) is a critical step in optoacoustic imaging, as it determines their optical and acoustic properties. Our quest to synthesize AuNRs with the desired parameters led us on a journey of experimentation and learning. While we ultimately opted to purchase AuNRs from Sigma-Aldrich [2] for our imaging experiments, our in-house synthesis efforts provided invaluable insights into the complexities of AuNR synthesis. In this chapter, we will delve into our synthesis attempts, highlighting the lessons learned and the knowledge gained from this valuable experience.

3.1 Determination of the type of Nanoparticle

The synthesis of high-quality gold nanoparticles (AuNRs) is paramount for achieving reliable optoacoustic imaging results. Our choice of particle type and synthesis conditions was guided by several critical factors:

- Absorption Peak: We opted for AuNRs with an absorption peak within the 700-900 nm range. This choice aligns with the spectral stability of our laser, which exhibits greater energy fluctuations at longer wavelengths.
- Peak Strength: A strong absorption peak is essential for eliciting a robust optoacoustic signal, enabling deeper tissue penetration and improved imaging capabilities.
- Particle Purity: We aimed for high purity AuNR samples, specifically a high ratio of nanorods to nanospheres. During the synthesis, spheres tend to elongate into rods over time, and the proportion of rods ultimately determines the overall signal strength.
- Narrow Peak Width: A narrow peak width, measured by the full-width-at-half-maximum (FWHM), is highly desirable for better distinguishing AuNRs from surrounding tissue.

3.2. Synthesis of the Gold Nanorods

Given these considerations, we investigated the synthesis of AuNRs [3][4] and gold bi-pyramidal nanoparticles (AuBPYs) [5][6]. AuBPYs exhibit optoacoustic properties comparable to AuNRs, and their FWHM is significantly narrower (see Figure 3.1). This narrow FWHM offers enhanced discrimination capabilities, making AuBPYs a promising alternative for optoacoustic imaging applications.

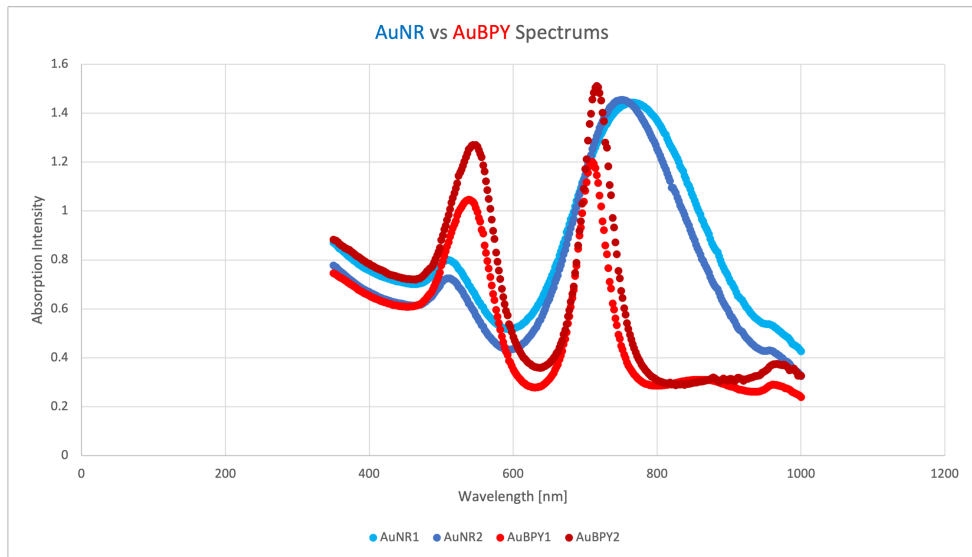


Figure 3.1: Comparison between AuNR and AuBPY Absorption Spectra

3.2 Synthesis of the Gold Nanorods

Given our prior experience with AuNRs, we initially aimed to continue using them for our optoacoustic imaging experiments. However, the employed AuNRs exhibited an absorption peak at around 1100 nm, making it challenging to accurately quantify the fluence applied to the particles due to the laser's spectral instability at higher wavelengths. To address this challenge, we sought to synthesize AuNRs with reduced peak absorption by lowering their aspect ratio. Aspect ratio, defined as the length of the particle divided by its width, is a key determinant of the peak absorption. We explored various seeded synthesis methods [3][4] to achieve this goal but, unfortunately, our efforts were unsuccessful. This setback prompted us to shift our focus to gold bi-pyramidal nanoparticles (AuBPYs).

3.3. Synthesis of the Bi-Pyramidal Nanoparticles

3.3 Synthesis of the Bi-Pyramidal Nanoparticles

Gold bi-pyramidal nanoparticles (AuBPYs) are less commonly used than AuNRs, and there is consequently less scientific literature available on their synthesis and properties. However, thanks to Daniil Nozdriukhin, a PhD student from the Razansky Lab at ETHZ, we were able to obtain valuable insights into AuBPY synthesis. He demonstrated that AuBPYs can be synthesized within the 700-900 nm range, and their peak absorption can be readily adjusted while maintaining the desirable optical and acoustic properties comparable to AuNRs (Figure 3.2).

Our synthesis approach followed a seeded method described in a published paper [5]. The procedure involves two solutions: the seed solution, containing the gold precursor, and the growth solution, which induces the growth of the gold nanoparticles from spherical into bi-pyramidal shapes.

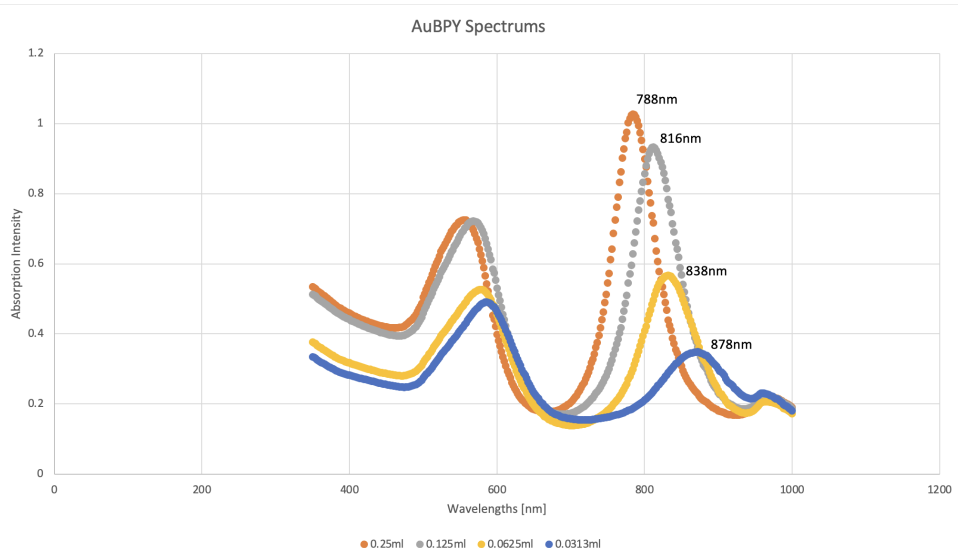


Figure 3.2: Spectrums of Different Absorption Peaks of AuBPY. Please take into consideration that the later AuBPY had less time to react to the growth solution, making their second peak lower than the first. We just wanted to show that that we can modify the peak absorption.

The amount of seed solution that we will put in the growth solution will influence the aspect ratio of the AuBPY as seen in Figure 3.2. So for example in the previously mentionned Figure3.2, if we put 0.25mL, we will have the peak absorption at 788nm and for 0.0625mL, we get 838nm. In addition, the FWHM is narrow which allows us to distinguish well the different aspect ratios of the AuBPY.

3.3. Synthesis of the Bi-Pyramidal Nanoparticles

3.3.1 Filtering

As expected, AuBPY synthesis does not yield a pure product, as some spherical nanoparticles remain unreacted to the growth solution. This low purity, denoted by the presence of residual spheres, gave us detrimental effects on the optoacoustic imaging performance. To achieve optimal results, we sought to remove these spheres from the final product. This would not only enhance the accuracy of SEM images but also reduce the first peak of absorption, which occurs at around 500 nm and is partially attributed to the spheres. Initially, we attempted to filter out the spheres as described in a published paper [5]. However, this method proved challenging due to particle aggregation, which significantly impaired their absorption properties, rendering them unusable. Due to time constraints, we ultimately decided to purchase AuNRs from Sigma-Aldrich [2]. This decision allowed us to obtain highly pure particles with predictable properties, streamlining the experimental process and ensuring reliable results for our optoacoustic imaging studies.

The purchased AuNRs possessed an absorption peak at 808 nm, perfectly aligned with our desired excitation wavelength range. Additionally, we obtained the gold concentration ($30\mu\text{g/mL}$) in the solution. Since the concentration could potentially impact the optoacoustic signal generation efficiency, we deemed it unnecessary to alter this concentration for our current study.

Chapter 4

Optoacoustic Setup

In this Chapter, we will discuss the experimental setup for lasering the gold nanoparticles. This setup is crucial for achieving accurate and reproducible results in optoacoustic imaging. A well-designed setup ensures that the laser beam is focused correctly on the nanoparticles, that the optical pulses are generated with the desired wavelength and duration, and that the acoustic signals generated by the nanoparticles are detected efficiently.

4.1 Laser Setup

To test our gold nanoparticles (AuNRs), we employed a pulsed near-infrared (NIR) laser that can be adjusted to emit light from 600 to 1200 nm. We attempted to use an open beam with a beam expander and a fiber to focus the laser beam onto the particles. The open beam with a beam expander resulted in a non-uniform beam, as shown in Figure 4.1b. This is because the laser itself does not output a uniform beam. Instead, we opted to use an optical fiber to get a more uniform beam, as seen in Figure 4.1a.

Optical fibers produce a Gaussian curve like beam which allows us to approximate the fluence that the particles receive. Using an optical fiber to direct the laser onto the AuNRs was essential for achieving uniform fluence and ensuring accurate and reproducible results in our optoacoustic imaging experiments.

To ensure consistent results and accurately assess the influence of laser-induced effects on the gold nanoparticles (AuNRs), it was crucial to approximate the fluence before each experiment. Fluence, defined as the amount of laser energy absorbed per unit area, can vary slightly due to minor changes in the lasered region. Measuring the laser's energy output with a powermeter at each wavelength provided a preliminary estimate (see Figure 5.3). However,

4.1. Laser Setup

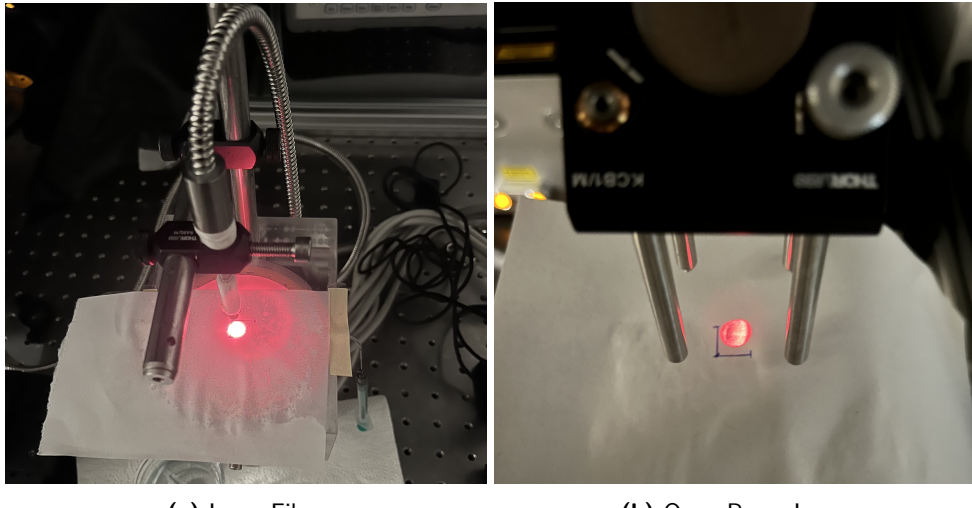


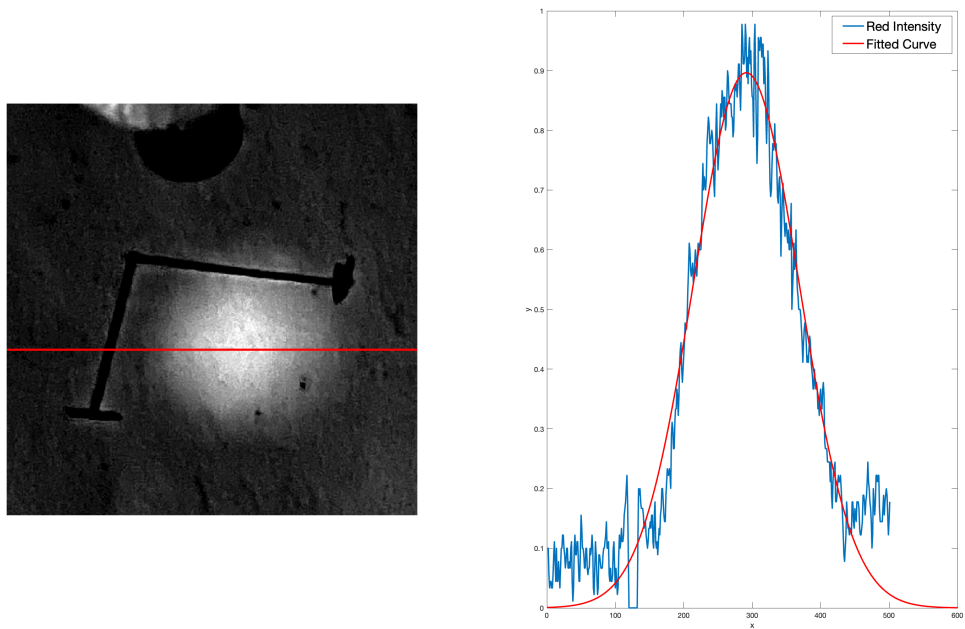
Figure 4.1: Comparison of how uniform the the laser fiber and open beam laser are

to achieve greater precision, we measured the Gaussian curve of the energy intensity, which revealed the distribution of laser energy across the beam.

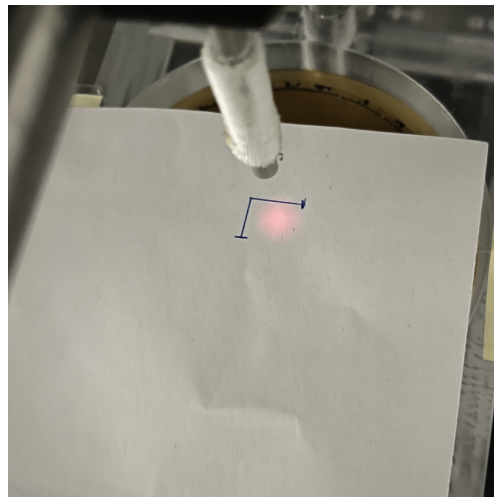
Estimating the illuminated surface was straightforward. We captured a 3-second averaged image of the laser beam with a scale, allowing us to approximate the diameter and calculate the surface area using the formula: $S = \pi(d/2)^2$. This calculation yielded an average surface area for the beam. However, as illustrated in Figure 4.2b, the beam profile exhibited non-uniformity. To refine our fluence estimate, we measured the point spread function (PSF) of the laser beam. The PSF provides a more precise representation of the laser's intensity distribution, allowing us to account for the non-uniform beam shape. As shown in Figure 4.2a, the PSF exhibited a Gaussian-like shape, validating our initial assumption.

By combining the measured laser energy, illuminated surface area, and PSF, we obtained a more accurate estimate of the fluence experienced by the AuNRs. This information was crucial for understanding the distribution of laser-induced effects within the tube where the nanoparticles were positioned.

4.2. Ultrasound Cup Setup



(a) Left: Cropped image of the laser with the line taken for the signal. Right: The Distribution of the laser intensity along the line.



(b) Image of the laser

Figure 4.2: Image of the Gaussian Distribution of the Laser

4.2 Ultrasound Cup Setup

To minimize the attenuation of the laser beam and ensure a consistent path for the ultrasound waves, we placed the cup with the agar medium at the opposite side of the laser. This arrangement allowed the laser beam to travel in air and the ultrasound waves propagated through an agar medium. This

4.2. Ultrasound Cup Setup

would minimize the attenuations.

For robust and reproducible testing, we employed a small plastic tube to deliver the AuNR solution. This approach ensured that we consistently tested the same volume of AuNRs at the same location, eliminating any variations due to differences in particle concentration or distribution. Additionally, using a tube made it easier to flush the tube and prepare it for the next sample and makes the computation faster and simpler since its spatial distribution will be the same for every experiment.

Another significant advantage of testing the AuNRs in a tube is that it eliminates the need to consider evaporation effects. When testing on a drop of AuNRs on a glass plate, the particles on the surface are prone to evaporation, which can significantly alter the particle concentration and affect the optoacoustic signals. By using a tube, we maintain a controlled environment and prevent particle evaporation, ensuring consistent results.

In summary, using a small plastic tube for AuNR delivery offers several benefits: consistent particle volume, simplified sample preparation, easier reconstruction of the signal and reduced particle evaporation, all contributing to more reliable and reproducible optoacoustic imaging experiments.

4.2. Ultrasound Cup Setup

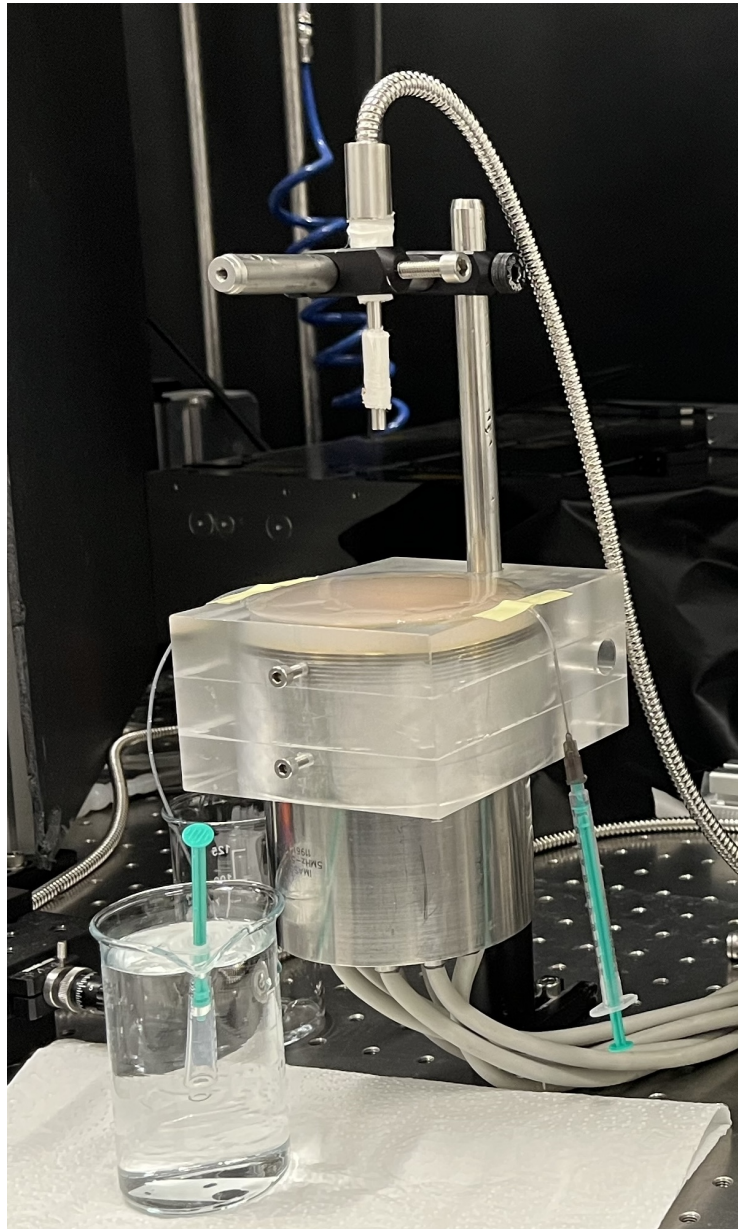


Figure 4.3: Complete View of the Setup, the fiber when lasering would be much closer to the tube

Chapter 5

Coding and Results

In this chapter, we will present our methods to model the decay of the signal of the AuNRs in function of different parameters. We will break down this process in multiple steps to make it as logical as possible.

5.1 Getting the Data

Our data acquisition process involved acquiring a 4D signal matrix by imaging the particles for 20 seconds with a specific energy and a specific wavelength. For each energy-wavelength combination, we followed a systematic approach to isolate the particle signal and extract its temporal behavior.

First, we averaged the signal matrix over time to obtain a 3D matrix representing the spatial distribution of particle signals. Next, we applied a threshold to identify the spatial coordinates of the particles within the tube. This step ensured that only the signal originating from the particles was considered for further analysis. We then set all non-particle coordinates to zero to eliminate irrelevant information.

Next, we employed the original data, masked the irrelevant coordinates from before, and averaged the remaining coordinates along the z-axis to generate a 3D matrix depicting the temporal evolution of the particle signal distribution within the tube (x, y, time).

To further analyze the particle signal, we approximated the tube as an ellipse, assuming the signal distribution mirrors the Gaussian light profile. The major axis of this ellipse represents the primary component of the particle signal and serves as a reference for our analysis, as shown in Figure 5.1. Along this axis, we assigned the different fluences, as illustrated in Figure 5.2. This approach allowed us to effectively increase the number of energy values considered in our experiments and to get more accurate energy values.

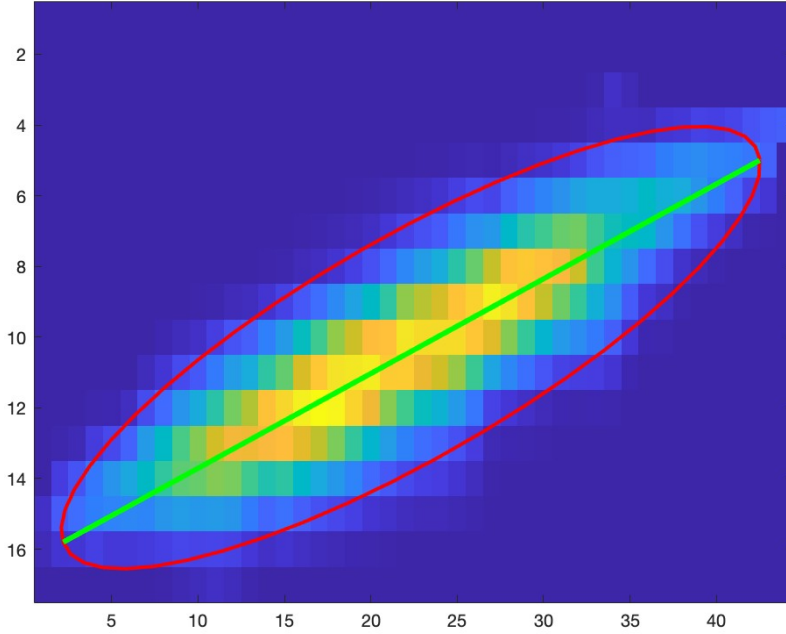


Figure 5.1: Signal of the Tube with the green line

Finally, we repeated this process for every wavelength and stitched all the wavelength-specific data together to obtain a 3D matrix that encapsulates the optoacoustic signal in function of wavelength, fluence, and time. This multidimensional matrix provides a comprehensive representation of the particle signal response under varying energy and wavelength conditions.

In addition to imaging the AuNRs, we would regularly monitor the laser's energy output using a powermeter, as shown in Figure 5.3.

To effectively visualize the acquired data, we averaged the observations across a specific variable and presented the resulting matrix in Figure 5.4. We deliberately included the initial 40 laser pulses from the analysis as they correspond to the laser's ramp-up phase, where the fluence is lower compared to subsequent pulses. However, during this initial phase, the nanoparticles have already begun to degrade, which is not incorporated into our modeling approach due to the complexity of estimating the fluence precisely.

Figure 5.4c clearly demonstrates the gradual degradation of the nanoparticles over increasing pulse numbers, as expected. Similarly, Figure 5.4a reveals a direct relationship between signal intensity and energy, with higher energy pulses leading to enhanced absorption. Notably, Figures 5.4a and 5.4b exhibit

5.1. Getting the Data

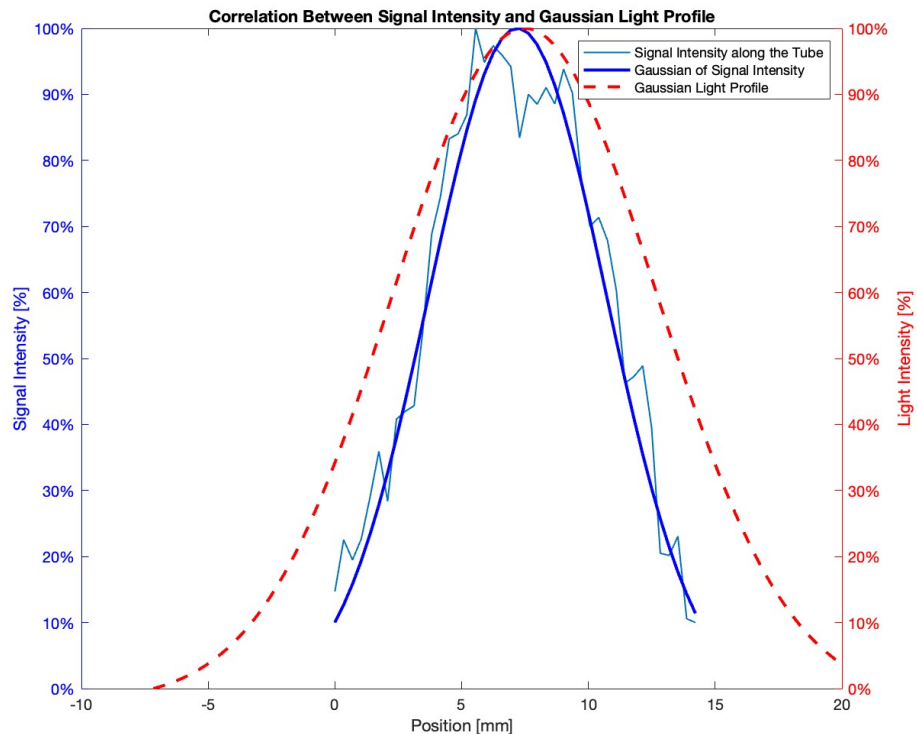


Figure 5.2: Signal profile with it's corresponding light intensity in red

a "barcode" pattern due to the assignment of zero signal intensity for energies not represented in the corresponding data.

5.2. Fitting the Data

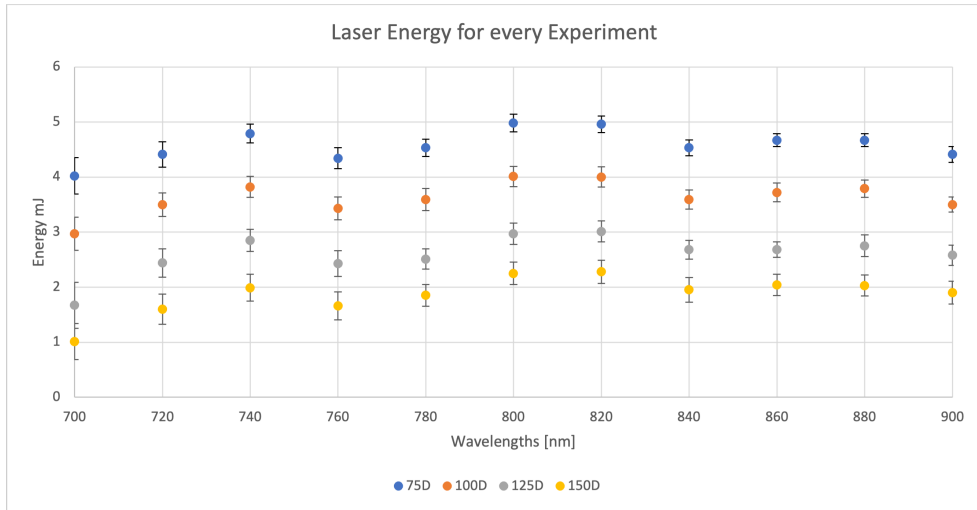


Figure 5.3: Energies of different Wavelengths and Delays of the Laser

5.2 Fitting the Data

Our modeling strategy involves a two-step approach:

- Denoising the Data: To better fit the data as we will do in the next step, smoothing out the data helps us get more consistent data.
- Degradation Modeling: We model the decay of the nanoparticles as a function of wavelengths and pulses at a constant energy. This is achieved by fitting an exponential decay function, $f = ae^{-b \cdot t}$, where a and b are the fitting parameters¹, and $t = p/10$ represents time (pulses divided by laser frequency).

The ultimate goal is to understand how wavelength and energy jointly influence the decay rate of the nanoparticles over time. We obtained an approximation of the decay rate of the original data, as depicted in Figure 5.5. This approximation serves as a valuable tool for analyzing the impact of wavelength and energy on nanoparticle degradation kinetics.

The effectiveness of our approximation method can be clearly seen in Figure 5.6, where the difference between the original and approximated data is mostly minimal. This indicates that our model accurately computed the decay coefficients of nanoparticle degradation.

¹The coefficients of both models can be found in the appendix

5.3. Results and Discussion

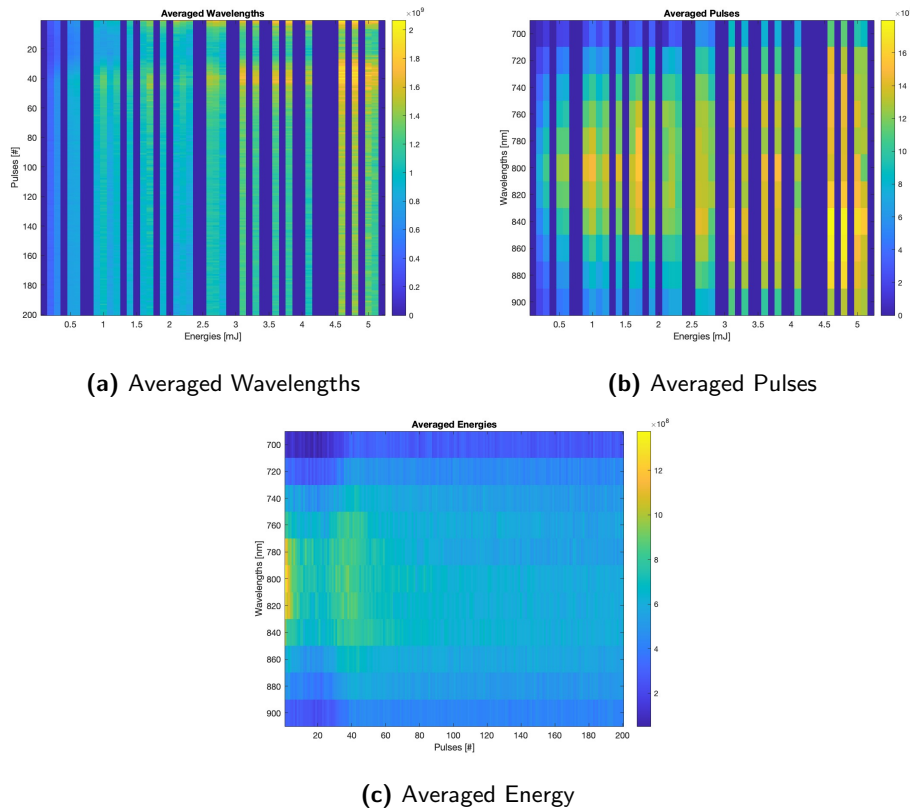


Figure 5.4: Representation of the matrix in function of Wavelengths, Pulses and Energy

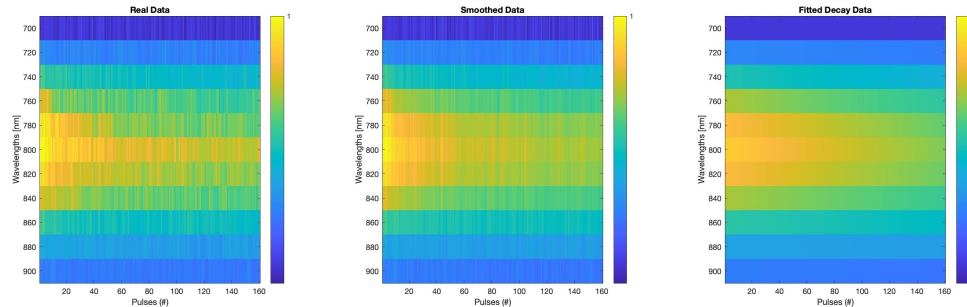


Figure 5.5: Visualization of the fitting of the original data

5.3 Results and Discussion

In this section, we present the results of our study and discuss the findings. Firstly, we extracted the coefficients from the exponential fitting of the data and calculated some statistical measures to measure the accuracy of our fitting as shown in Figure 5.7

5.3. Results and Discussion

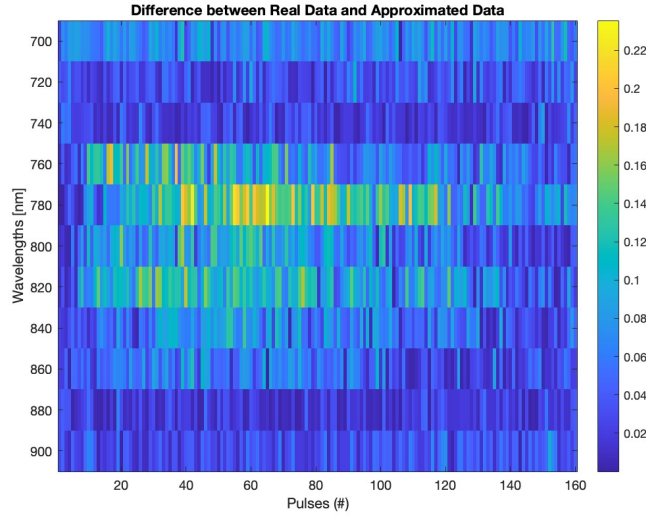


Figure 5.6: Absolute Error between Real Data and Approximated Data

Secondly, we evaluated the degradation of the signal intensity relative to its initial value after 16 seconds as a function of wavelength (Figure 5.8).

This analysis revealed an interesting trade-off between signal intensity and degradation rate. For instance, if the goal is to achieve a relatively short signal lifetime with high intensity, wavelengths between 740 and 840nm would be preferable.

Next, we investigated the influence of laser energy on the signal intensity. To assess this dependence, we compared the signal intensity at different laser delays. Figure 5.9 illustrates the relative increase in laser energy per delay per wavelength.

Comparing the signal intensity gain (Figure 5.10) to the increasing laser energy, it becomes evident that in certain instances, such as at 800 nm, an increase in energy provides minimal benefit as the nanoparticles will degrade regardless.

Even though the results are promising, some improvements can be made by including these factors in the model:

- **Laser Ramp-Up:** The initial ramp-up phase of the laser significantly degrades the gold nanorods (AuNRs) before the actual imaging process begins. This premature degradation affects the optoacoustic signal and introduces inconsistencies in the data.
- **Laser Fluctuation:** The laser itself fluctuates in energy, further contributing to the variability of the optoacoustic signal. This fluctuation makes it challenging to establish a stable and reliable baseline for comparison.

5.3. Results and Discussion

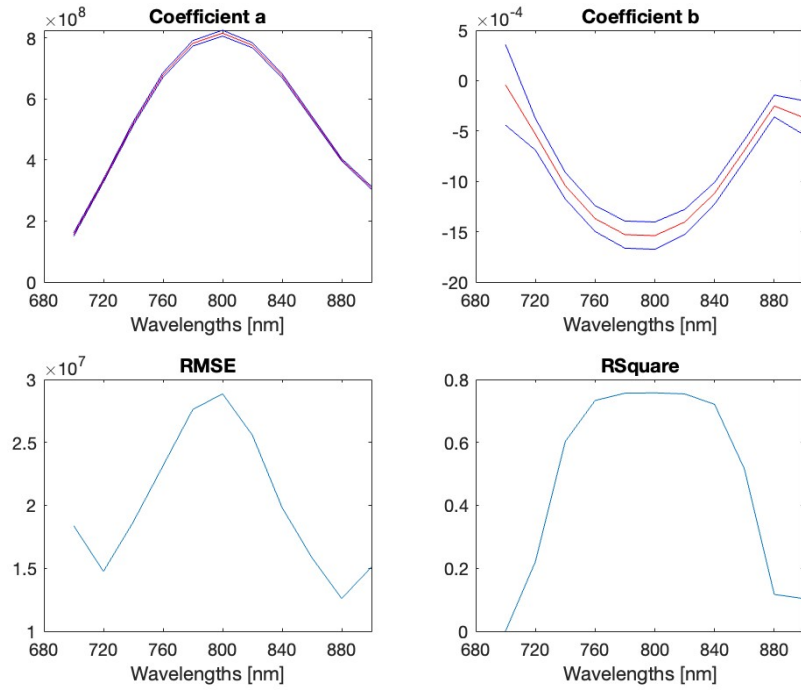


Figure 5.7: Coefficients of Decay for the function $f = ae^{-b \cdot p/10}$

- AuNR Agglomeration: The AuNRs can agglomerate, or clump together, during the imaging process. This agglomeration can alter the optical properties of the nanoparticles and distort the optoacoustic signal.

5.3. Results and Discussion

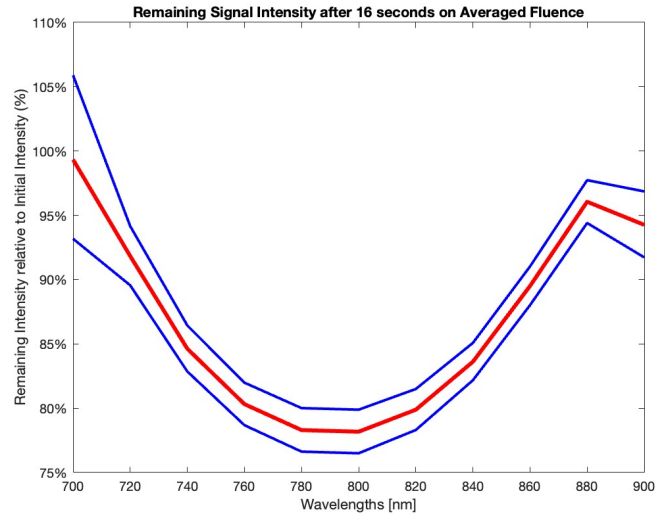


Figure 5.8: Signal Intensity Decay after 16 seconds with 90% confidence Intervals

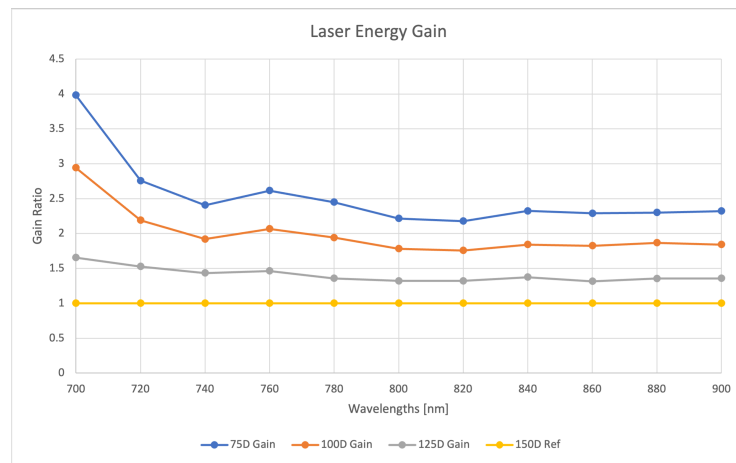


Figure 5.9: Laser Energy gain compared to the lowest Delay

5.3. Results and Discussion

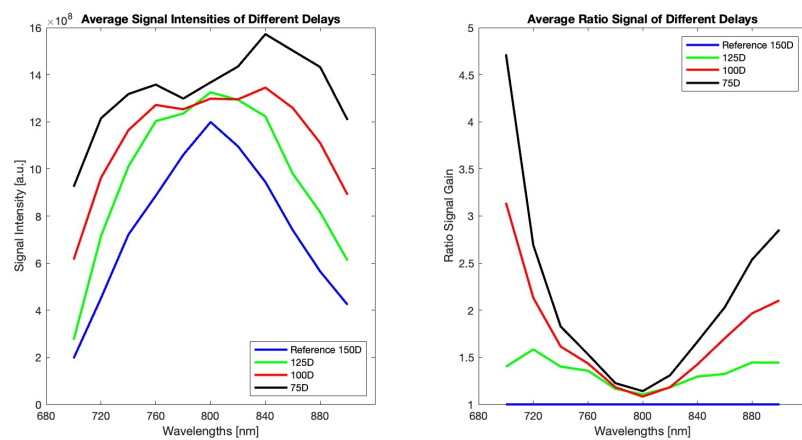


Figure 5.10: Signal Intensity gain compared to the lowest Signal Intensity

Chapter 6

SEM Imaging analysis

To further our understanding of the AuNRs' OA signal decay process and gain insights into their behavior during imaging, we developed a comprehensive application to segment particles in SEM images. This application leverages image processing techniques to detect, classify, and measure particles within images, enabling us to visualize the morphological changes of AuNRs as they decay. The application's intuitive interface and straightforward functionalities empower us to streamline the analysis of SEM images, providing a valuable tool for exploring the intricate dynamics of AuNRs in the optoacoustic imaging setting.

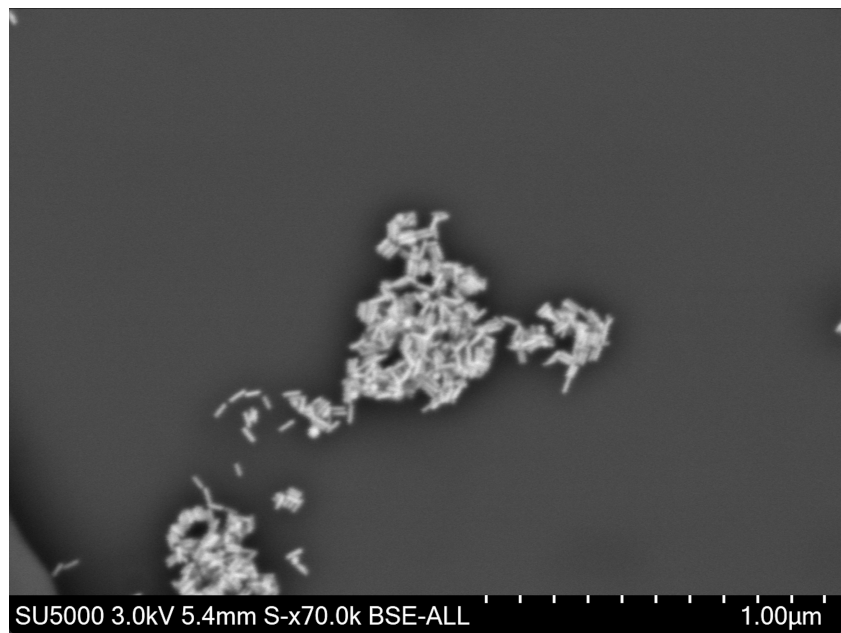


Figure 6.1: Example of an Image that can be processed by the app

6.1 Particle Detector App

This application is designed to streamline the process of particle detection and analysis in images. It provides a user-friendly interface and a set of functionalities that enable efficient processing of images to identify and quantify particles. The application's functionalities are accessible through a sidebar menu, providing clear navigation and a seamless user experience.

The functionalities include:

- **See Image Results:** This functionality allows the user to view the results of particle detection for a specific image. The user can identify individual particles, measure their properties, and obtain detailed insights into the particle distribution within the image.
- **Process Particles:** This central functionality enables the user to process an image to detect and analyze particles. The application employs advanced algorithms to identify particle boundaries, measure particle dimensions, and label the particles according to their characteristics.
- **See All Results:** This functionality provides a comprehensive overview of the results from all processed images. The user can easily navigate through the results and gain a complete understanding of the particle distribution patterns.

6.2 Image Processing

The Particle Detector App commences the analysis process by converting the selected image into a grayscale format, facilitating the subsequent thresholding step. To reduce noise, a Gaussian blur filter is applied. This step ensures that the thresholding process isolates the particle boundaries without being influenced by fine details.

Thresholding: A critical aspect of particle detection is accurately distinguishing particles from the background of the image. The application employs a thresholding technique to achieve this distinction. A user-adjustable threshold value is applied to the grayscale image, converting it into a binary image. Contours, representing the outlines of potential particles, are identified within the binary image.

Minimum Area Rectangle and DataFrame: For each detected contour, the application identifies the minimum area rectangle that encloses it. This rectangle serves as a representation of the particle's outline. The properties of these rectangles, including their area, major axis, minor axis, and centroid coordinates, are extracted and stored in a matrix.

Particle Classification: The application facilitates the classification of detected particles into four categories: rods, spheres, other, and noise. The user can

6.3. Results of SEM Analysis

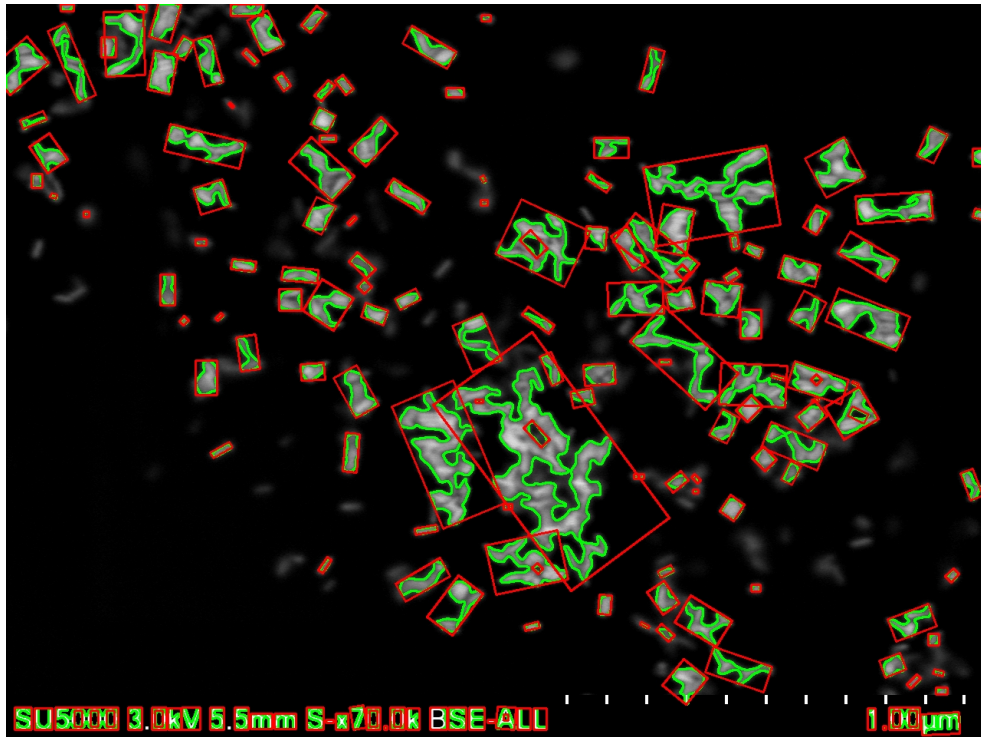


Figure 6.2: Example of a Thresholded Image, in red are the contour boxes and in green the encircled object.

seamlessly navigate through the particles and classify each particle based on its morphology. The classification of each particle is stored in the matrix.

6.3 Results of SEM Analysis

In addition to evaluating the optoacoustic signal, we also explored how imaging influenced the physical properties of AuNRs. To investigate this, we imaged AuNRs under five different conditions by varying the wavelength, energy, and exposure time to the laser, and then acquired scanning electron microscopy (SEM) images of them. Subsequently, we employed the application to measure the major and minor axis lengths of the nanoparticles. The overall results of this image processing are presented in Figure 6.3.

To further investigate the potential relationships between imaging conditions and AuNR morphology, we plotted the major versus minor axis lengths for the particles altogether, as shown in Figures 6.4. We observed some degradation of the AuNRs, however the accuracy could be improved. This could be attributed to the limitations of SEM imaging, which may not provide sufficient resolution to precisely determine the boundaries of AuNRs. Alternatively, the agglomeration of rods during imaging could disrupt their

6.3. Results of SEM Analysis

Name	# of Rods	Major Axis	Minor Axis	Aspect Ratio	# of Spheres	Major Axis	Minor Axis	Aspect Ratio
700nm 3mJ 10s	26	43.36	16.53	2.62	12	42.74	36.49	1.17
800nm 4mJ 10s	3	38.56	13.55	2.85	0	-	-	-
900nm 3.5 mJ 10s	24	39.03	13.79	2.83	12	31.32	24.82	1.26
800nm 3mJ 5s	17	40.98	17.42	2.35	9	38.36	29.63	1.29
800nm 2.3mJ 5s	4	50.42	21.24	2.37	2	32.88	21.45	1.53
800nm 4mJ 60s	0	-	-	-	0	-	-	-
Total	74	41.59	15.98	2.62	35	37.13	34.99	1.25

Figure 6.3: Table of the findings in the SEM Images, the name describes the wavelength used (number before nm), energy (before the mJ) and the duration (before s) of the laser.

characteristic rod-like shape, making it challenging to accurately measure their dimensions.

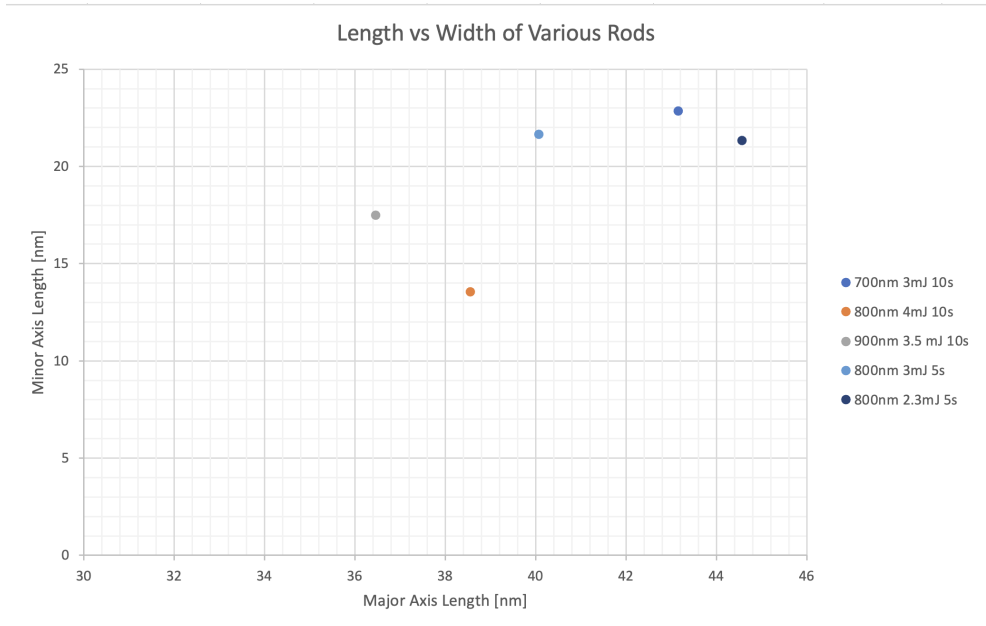


Figure 6.4: Major vs Minor Axis Length of Particles for Different Imaging Properties

6.3. Results of SEM Analysis

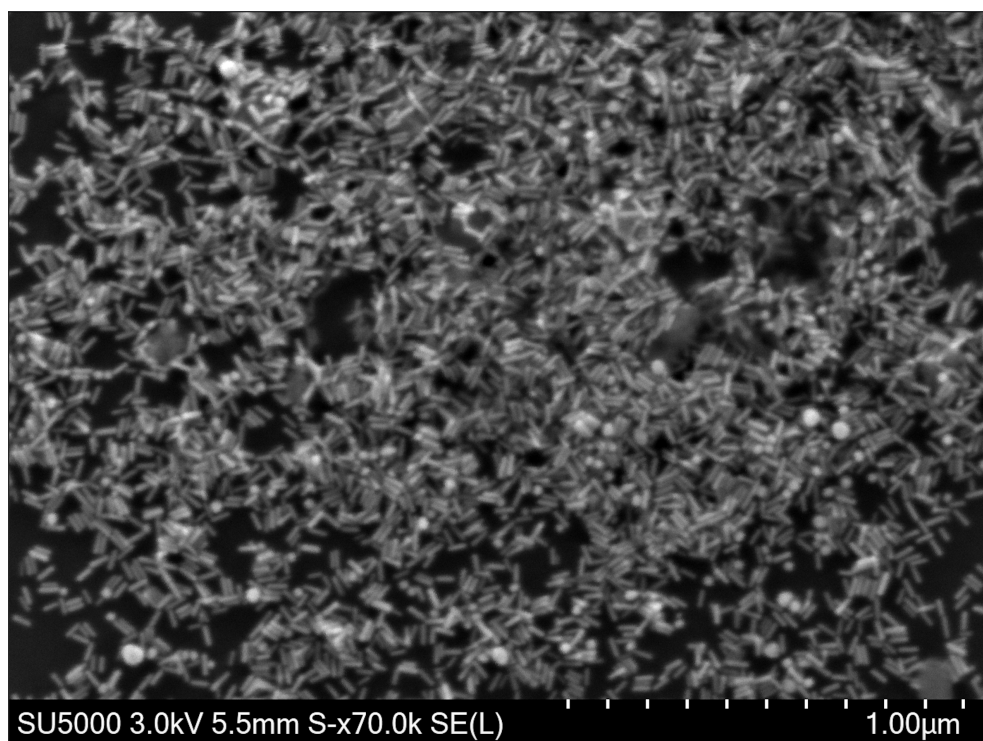


Figure 6.5: Example of Agglomerated AuNRs

Chapter 7

Conclusion

This bachelor thesis successfully developed a novel method for quantifying the OA signal decay of gold nanorods (AuNRs). We presented the results of the degradation of gold nanorod (AuNR) signal intensity over time and its correlation with laser energy and wavelength. We found that we can approximate the signal intensity decays exponentially with time. This innovative approach paves the way for more accurate and efficient assessments of AuNR degradation.

Additionally, we created a software program capable of segmenting AuNRs in scanning electron microscopy (SEM) images and determining their physical dimensions. We investigated the influence of imaging conditions on the physical properties of gold nanorods (AuNRs) by varying the wavelength, energy, and exposure time of the laser used for imaging. They observed some degradation of the AuNRs, but the accuracy of their measurements could be improved due to limitations in SEM imaging resolution or the agglomeration of rods during imaging.

With further refinement and innovation, these methods hold immense potential to transform into sophisticated and highly accurate tools for analyzing the decay of AuNRs, revolutionizing our understanding of these remarkable nanoparticles.

Bibliography

- [1] *Course: 227-0384-00L Ultrasound Fundamentals and Applications in Biology and Medicine HS2023 — Moodle Course.* [Online]. Available: <https://moodle-app2.let.ethz.ch/course/view.php?id=20574> (visited on 12/30/2023).
- [2] *Gold-Nanostäbchen 10 nm diameter, silica coated, max, 850 nm, dispersion in H₂O — Sigma-Aldrich, de.* [Online]. Available: <http://www.sigmaaldrich.com/> (visited on 12/30/2023).
- [3] D. Xu, J. Mao, Y. He, and E. S. Yeung, "Size-tunable synthesis of high-quality gold nanorods under basic conditions by using H₂O₂ as the reducing agent," en, *Journal of Materials Chemistry C*, vol. 2, no. 25, pp. 4989–4996, Jun. 2014, Publisher: The Royal Society of Chemistry, ISSN: 2050-7534. doi: [10.1039/C4TC00483C](https://doi.org/10.1039/C4TC00483C). [Online]. Available: <https://pubs.rsc.org/en/content/articlelanding/2014/tc/c4tc00483c> (visited on 12/30/2023).
- [4] Y. Guo *et al.*, "Spectrum and size controllable synthesis of high-quality gold nanorods using 1,7-dihydroxynaphthalene as a reducing agent," en, *Dalton Transactions*, vol. 52, no. 4, pp. 1052–1061, Jan. 2023, ISSN: 1477-9234. doi: [10.1039/D2DT03646K](https://doi.org/10.1039/D2DT03646K). [Online]. Available: <https://pubs.rsc.org/en/content/articlelanding/2023/dt/d2dt03646k> (visited on 12/30/2023).
- [5] Q. Li, X. Zhuo, S. Li, Q. Ruan, Q.-H. Xu, and J. Wang, "Production of Monodisperse Gold Nanobipyramids with Number Percentages Approaching 100% and Evaluation of Their Plasmonic Properties," en, *Advanced Optical Materials*, vol. 3, no. 6, pp. 801–812, 2015, eprint: <https://onlinelibrary.wiley.com/doi/pdf/10.1002/adom.201400505>, ISSN: 2195-1071. doi: [10.1002/adom.201400505](https://doi.org/10.1002/adom.201400505). [Online]. Available: <https://onlinelibrary.wiley.com/doi/abs/10.1002/adom.201400505> (visited on 12/30/2023).

Bibliography

- [6] J.-H. Lee, K. J. Gibson, G. Chen, and Y. Weizmann, "Bipyramid-templated synthesis of monodisperse anisotropic gold nanocrystals," en, *Nature Communications*, vol. 6, no. 1, p. 7571, Jun. 2015, Number: 1 Publisher: Nature Publishing Group, ISSN: 2041-1723. doi: 10.1038/ncomms8571. [Online]. Available: <https://www.nature.com/articles/ncomms8571> (visited on 12/30/2023).

Declaration of originality

The signed declaration of originality is a component of every semester paper, Bachelor's thesis, Master's thesis and any other degree paper undertaken during the course of studies, including the respective electronic versions.

Lecturers may also require a declaration of originality for other written papers compiled for their courses.

I hereby confirm that I am the sole author of the written work here enclosed and that I have compiled it in my own words. Parts excepted are corrections of form and content by the supervisor.

Title of work (in block letters):

Authored by (in block letters):

For papers written by groups the names of all authors are required.

Name(s):

First name(s):

With my signature I confirm that

- I have committed none of the forms of plagiarism described in the '[Citation etiquette](#)' information sheet.
- I have documented all methods, data and processes truthfully.
- I have not manipulated any data.
- I have mentioned all persons who were significant facilitators of the work.

I am aware that the work may be screened electronically for plagiarism.

Place, date

Signature(s)

For papers written by groups the names of all authors are required. Their signatures collectively guarantee the entire content of the written paper.